Rayleigh–Taylor instability of reaction-diffusion acidity fronts

J. Yang, A. D'Onofrio, S. Kalliadasis, and A. De Wit

Citation: The Journal of Chemical Physics **117**, 9395 (2002); doi: 10.1063/1.1516595
View online: http://dx.doi.org/10.1063/1.1516595
View Table of Contents: http://scitation.aip.org/content/aip/journal/jcp/117/20?ver=pdfcov
Published by the AIP Publishing

Rayleigh–Taylor instability of reaction-diffusion acidity fronts

J. Yang
Department of Chemical Engineering, University of Leeds, Leeds, LS2 9JT, United Kingdom

A. D'Onofrio
Service de Chimie Physique and Centre for Nonlinear Phenomena and Complex Systems, CP 231, Université Libre de Bruxelles, 1050 Brussels, Belgium

S. Kalliadasis
Department of Chemical Engineering, University of Leeds, Leeds, LS2 9JT, United Kingdom

A. De Wit[a)]
Service de Chimie Physique and Centre for Nonlinear Phenomena and Complex Systems, CP 231, Université Libre de Bruxelles, 1050 Brussels, Belgium

(Received 20 February 2002; accepted 30 August 2002)

We consider the buoyancy driven Rayleigh–Taylor instability of reaction-diffusion acidity fronts in a vertical Hele–Shaw cell using the chlorite–tetrathionate (CT) reaction as a model system. The acid autocatalysis of the CT reaction coupled to molecular diffusion yields isothermal planar reaction-diffusion fronts separating the two miscible reactants and products solutions. The reaction is triggered at the top of the Hele–Shaw cell and the resulting front propagates downwards, invading the fresh reactants, leaving the product of the reaction behind it. The density of the product solution is higher than that of the reactant solution, and hence a hydrodynamic instability develops due to unfavorable density stratification. We examine the linear stability of the isothermal traveling wavefront with respect to disturbances in the spanwise direction and demonstrate the existence of a preferred wavelength for the developed fingering instability. Our linear stability analysis is in excellent agreement with two-dimensional numerical simulations of the fully nonlinear system.
 [DOI: 10.1063/1.1516595]

I. INTRODUCTION

Hydrodynamic deformations of interfaces between two reactive fluids as well as flows induced by chemical reactions at the front between two initially motionless fluids are encountered frequently in petroleum, chemical, and pharmaceutical engineering. The spatiotemporal dynamics resulting from the interplay between hydrodynamics and chemical reactions can easily become rather complex as a number of effects such as viscosity or density variations, surface tension, or heat effects may come into play. In that respect, the fundamental understanding of the dynamics of reactive fluids can benefit from simple model systems in which only some of the possible sources of instability are present.

Isothermal, buoyantly unstable, autocatalytic chemical fronts are one such model system which can be used as a prototype to study the effects of the coupling between chemical reactions and Rayleigh–Taylor type of hydrodynamic instabilities. Rayleigh–Taylor instabilities occur whenever fluids of different density are subject to acceleration in a direction opposite to that of the density gradient.[1] Such a situation is encountered when chemical fronts separate a denser solution lying on top of a lighter one in the gravity field. The initially planar fronts resulting from the coupling between nonlinear chemical kinetics and diffusion[2–4] lose then stability due to buoyancy effects which induce a cellular fingering deformation of the front. Such an instability has been observed, for instance, in the iodate–arsenious acid (IAA) reaction, a redox reaction known to produce a decrease of density during the course of the reaction. Hence, upwards traveling IAA fronts become unstable to buoyancy effects and a deformation of the front is indeed observed. Numerous experimental[2,5,6] as well as theoretical works[7–10] have been devoted to the study of convective deformations of IAA fronts (mainly in capillary tubes). More recent works have further analyzed fingering of such IAA fronts in laterally extended Hele–Shaw cells (two glass plates separated by a small gap width) in which several convection rolls can appear.[11–15] The main advantages of the IAA system as a prototype to study the coupling of hydrodynamics with kinetics/diffusion are that density changes due to heat effects are negligible in the geometries considered. In addition, a simple one-variable model describing the evolution of iodide concentration[16–18] is available and remains valid for the concentration ranges considered in the experiments.[18] Experimental studies have also been performed with other buoyantly unstable miscible reaction-diffusion waves[2,19–22] including the chlorite–thiourea and free-radical polymerization reactions. Unlike the IAA system, however, heat effects in those fronts are no longer negligible and must be taken into account in the theoretical analysis.[2,23–25] It is then desirable to analyze another chemical system that provides unstable fronts between miscible solutions of different densities and for which heat effects can be safely neglected. The aim

[a)]Electronic mail: adewit@ulb.ac.be

is to understand to what extent the stability properties of chemical fronts and the resulting nonlinear dynamics are kinetics dependent. In particular, it would be of interest to compare with the IAA system and to establish the instability features which are model dependent.

Here, we focus on the Rayleigh–Taylor instability of reaction-diffusion acidity fronts using the chlorite–tetrathionate (CT) reaction as a model system. In this redox reaction involving the chlorite oxidation of tetrathionate,[26] a hydrodynamic instability of Rayleigh–Taylor type develops when the reaction front propagates downwards, since the density of the reaction increases in the course of the reaction. The CT system is known to produce bistability in continuously stirred reactors. When diffusion comes into play, the CT reaction can exhibit oscillatory and traveling waves[27–30] as well as spatial bistability.[29] It was also the first acid-catalyzed reaction used to study diffusive instabilities of chemical fronts.[30–33] The diffusive destabilization of the front occurs because of differential diffusivity of the activator and inhibitor species involved in the nonlinear kinetics leading eventually to a cellular deformation of the front.[34–36] In particular, a diffusive instability occurs when the activator (here the protons) diffuses slower than the inhibitor (here tetrathionate ions), which is experimentally achieved by binding the hydrogen ions to immobilized carboxylate groups.[31] Here, we assume that there is no such binding, and hence the diffusivity of the protons is larger than or equal to the diffusivity of the tetrathionate ions, thus excluding the possibility of a diffusive destabilization of the front. Hence, we focus on the hydrodynamic fingering instability of the front arising because of density differences between the reactant and product solutions. In the particular case that the two species have the same diffusivities, the two-variable model can be reduced to a one-variable (fourth-order) model. This allows us to compare with the IAA system in order to establish the instability features which are kinetics dependent. The framework developed here can be readily used to explore other two-variable systems.

In Sec. II, we formulate the model of the convection–reaction-diffusion CT system in the geometry of a Hele–Shaw cell. In Sec. III we construct the base state of the system which is a planar traveling front in a moving frame. In Sec. IV we perform a linear stability analysis of this front with respect to infinitesimal disturbances in the spanwise direction—such disturbances arise because of buoyancy effects. We obtain the dispersion relation for the growth rate of these disturbances as a function of wave number for different values of the governing dimensionless parameters. We demonstrate that small amplitude disturbances in the spanwise direction are linearly unstable for small wave numbers—with a band of unstable wave numbers that extends to zero—and stable for long wave numbers. Section V compares the results of the linear stability analysis of Sec. IV with numerical simulations of the fully nonlinear system. Finally, in Sec. VI we contrast the stability properties of CT and IAA fronts and we conclude with suggestions for future work in the problem of density fingering of chemical fronts.

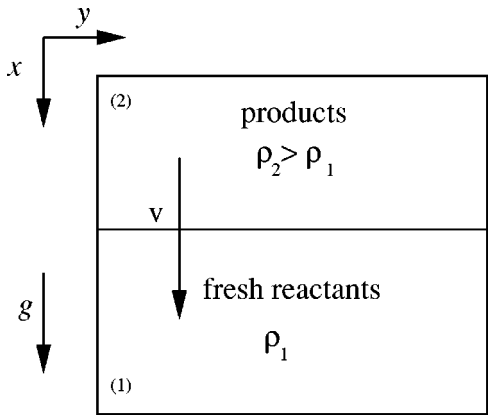

FIG. 1. Geometry of the CT system in a Hele–Shaw cell.

II. MODEL

Our system is a two-dimensional Hele–Shaw cell of size $L_x \times L_y$ with the gravity field along the x direction (the geometry is depicted in Fig. 1). The cell is filled with the reactants of the CT reaction. The reaction is triggered at the top of the cell. The resulting chemical front moves downwards with velocity v invading the fresh reactants, chlorite $[ClO_2^-]$ and tetrathionate $[S_4O_6^{2-}]$, leaving the product $[H^+]$ of the reaction behind it according to the overall stoechiometric reaction[26]

$$7ClO_2^- + 2S_4O_6^{2-} + 6H_2O \rightarrow 7Cl^- + 8SO_4^{2-} + 12H^+.$$

The density of the product solution, ρ_2, is higher than that of the reactant solution, ρ_1. Hence, the downwards traveling chemical front is buoyantly unstable and develops density fingers as time progresses. Our objective here is to study the stability of the planar reaction-diffusion front with respect to the hydrodynamic buoyancy effects.

The starting point of our analysis is the assumption that the fluid in the Hele–Shaw cell is incompressible and the velocity field $\underline{u}$ for a given pressure gradient $\underline{\nabla} p$ can be obtained using Darcy's law.[37,38] The CT acid catalyzed reaction taking place in slight excess of chlorite is described by a simple two-variable reaction-diffusion model[28,33] for the two main species of the CT reaction, i.e., $\alpha = [S_4O_6^{2-}]$ and $\beta = [H^+]$. These two reaction-diffusion equations are coupled to the flow field through an advection term. The governing dimensional equations are then

$$\underline{\nabla} \cdot \underline{u} = 0, \tag{1}$$

$$\underline{\nabla} p = -\frac{\mu}{K}\underline{u} + \rho(\alpha,\beta)\underline{g}, \tag{2}$$

$$\frac{\partial \alpha}{\partial t} + \underline{u} \cdot \underline{\nabla} \alpha = D_\alpha \nabla^2 \alpha - r, \tag{3}$$

$$\frac{\partial \beta}{\partial t} + \underline{u} \cdot \underline{\nabla} \beta = D_\beta \nabla^2 \beta + 6r, \tag{4}$$

where the viscosity μ and the permeability $K = a^2/12$ are constant in space and time, with a being the gap width of the

Hele–Shaw cell. D_α and D_β are the diffusion coefficients of tetrathionate ions and protons, respectively. The dimensional reaction rate r is given by

$$r = q\{2[\mathrm{ClO}_2^-]_0 + 7(\alpha - \alpha_0)\}\alpha\beta^2, \tag{5}$$

where $\alpha_0 \equiv \alpha|_{t=0}$ and q is the reaction rate constant of the overall reaction. Here, we assume that the dependence of the density of the solution on the solute concentration appears only in the gravity term of Darcy's law (Boussinesq approximation). Therefore, the density ρ of the solution is a function of α and β, i.e., $\rho = \rho(\alpha,\beta)$. For α, $\beta \ll 1$, a Taylor series expansion at $(\alpha,\beta)=(0,0)$ up to O(2) yields

$$\rho = \rho_0 + \gamma_1\alpha + \gamma_2\beta, \tag{6}$$

where ρ_0 is the density of the fluid in the absence of reactants (e.g., water) with $\gamma_1 = \partial\rho/\partial\alpha|_{\alpha,\beta=0}$ and $\gamma_2 = \partial\rho/\partial\beta|_{\alpha,\beta=0}$. We notice that, strictly speaking, ρ depends on the concentration of all species of the CT reaction but the stoichiometry and simple conservation arguments allow us to express it as a function of α and β only. The density of the reactant solution (phase 1) is then $\rho_1 = \rho_0 + \gamma_1\alpha_0$, while the density of the product solution (phase 2) is simply $\rho_2 = \rho_0 + \gamma_2\beta_0$, where β_0 is the product concentration when the reaction is complete, i.e., the concentration of β far behind the front. Hence, for the heavy fluid to be on top of the light fluid (unfavorable density stratification) we must have $\rho_2 > \rho_1$ or $\gamma_2\beta_0 > \gamma_1\alpha_0$. We shall demonstrate later on that $\beta_0 = 6\alpha_0$ and therefore $\gamma_2 > \gamma_1/6$ for instability.

To balance viscous and buoyancy forces, we introduce a characteristic velocity U defined from

$$U = \frac{\Delta\rho g K}{\nu}, \tag{7}$$

where $\Delta\rho = (\rho_2 - \rho_1)/\rho_0$ and $\nu = \mu/\rho_0$ is the kinematic viscosity. In addition, balancing convection to diffusion (as there is no characteristic length or time in our problem) suggests the following characteristic hydrodynamic length and time scales:

$$L_h = \frac{D_\alpha}{U}; \quad \tau_h = \frac{D_\alpha}{U^2}. \tag{8}$$

We then nondimensionalize Eqs. (1)–(4) by scaling velocity, length, and time by U, L_h, and τ_h, respectively. Pressure, density, and concentrations α, β are scaled by $\mu D_\alpha/K$, $(\rho_2 - \rho_1)$, and α_0, respectively. Equations (1)–(4) then become

$$\underline{\nabla}\cdot\underline{u}' = 0, \tag{9}$$

$$\underline{\nabla}p' = -\underline{u}' + \rho'\underline{i}_x, \tag{10}$$

$$\frac{\partial\alpha'}{\partial t} + \underline{u}'\cdot\underline{\nabla}\alpha' = \nabla^2\alpha' - r', \tag{11}$$

$$\frac{\partial\beta'}{\partial t} + \underline{u}'\cdot\underline{\nabla}\beta' = \delta\nabla^2\beta' + 6r', \tag{12}$$

$$\rho' = \rho_0' + \gamma_1'\alpha' + \gamma_2'\beta', \tag{13}$$

where the primes denote dimensionless variables, $\delta = D_\beta/D_\alpha$, $\gamma_1' = \gamma_1\alpha_0/(\rho_2 - \rho_1)$, $\gamma_2' = \gamma_2\alpha_0/(\rho_2 - \rho_1)$, and $\underline{i}_x$ the unit vector in the streamwise direction. The dimensionless rate law now reads

$$r' = \frac{D_\alpha}{U^2} q\alpha_0^3\alpha'\beta'^2(\kappa + 7\alpha'), \tag{14}$$

with $\kappa = 2[\mathrm{ClO}_2^-]_0/\alpha_0 - 7$. In addition, we define the characteristic chemical time scale as

$$\tau_c = \frac{1}{q\alpha_0^3}, \tag{15}$$

and hence we introduce the Damköhler number, *Da*, as the ratio of the hydrodynamic to the chemical time scale, i.e.,

$$Da = \frac{\tau_h}{\tau_c} = \frac{D_\alpha}{U^2} q\alpha_0^3. \tag{16}$$

Finally, we define a hydrostatic pressure gradient from

$$\underline{\nabla}p'' = \underline{\nabla}p' - \rho_0'\underline{i}_x. \tag{17}$$

Combining Eqs. (9)–(14), (16), (17), and dropping all primes, yields the basic equations for the analysis to follow:

$$\underline{\nabla}\cdot\underline{u} = 0, \tag{18}$$

$$\underline{\nabla}p = -\underline{u} + (\gamma_1\alpha + \gamma_2\beta)\underline{i}_x, \tag{19}$$

$$\frac{\partial\alpha}{\partial t} + \underline{u}\cdot\underline{\nabla}\alpha = \nabla^2\alpha - Daf(\alpha,\beta), \tag{20}$$

$$\frac{\partial\beta}{\partial t} + \underline{u}\cdot\underline{\nabla}\beta = \delta\nabla^2\beta + 6Daf(\alpha,\beta), \tag{21}$$

with

$$f(\alpha,\beta) = \alpha\beta^2(\kappa + 7\alpha). \tag{22}$$

III. BASE STATE: TRAVELING FRONT SOLUTION

We now construct the base state of the system in the form of a planar traveling wavefront. Multiplying (20) by 6 and adding the resulting equation to (21) gives

$$\frac{\partial(\beta + 6\alpha)}{\partial t} + \underline{u}\cdot\underline{\nabla}(\beta + 6\alpha) = \nabla^2(\delta\beta + 6\alpha), \tag{23}$$

and the system is now described by (18)–(23). We seek a permanent-form traveling wave solution (α_s,β_s) of these equations in the absence of convection. By setting $\underline{u} = \underline{0}$ and introducing the moving coordinate $z = x - ct$ with c the speed of the traveling wave, we obtain

$$-c\frac{d\alpha_s}{dz} = \frac{d^2\alpha_s}{dz^2} - Daf(\alpha_s,\beta_s), \tag{24a}$$

$$-c\frac{d\beta_s}{dz} = \delta\frac{d^2\beta_s}{dz^2} + 6Daf(\alpha_s,\beta_s), \tag{24b}$$

$$-c\frac{d(\beta_s + 6\alpha_s)}{dz} = \frac{d^2(\delta\beta_s + 6\alpha_s)}{dz^2}. \tag{24c}$$

Integrating (24c) once, we get $-c(\beta_s + 6\alpha_s) = (d/dz)(\delta\beta_s + 6\alpha_s) + c_0$, where c_0 is the integration constant which can

be determined from the boundary condition $\alpha_s \to 1$, $\beta_s \to 0$ as $z \to +\infty$, or $c_0 = -6c$. The resulting equation can then be integrated once more to give

$$\beta_s = -\frac{6}{\delta}\alpha_s + \frac{6}{\delta}e^{-(c/\delta)z}\left(\frac{1}{\delta}-1\right)\int \alpha_s e^{(c/\delta)z}dz + 6 + \frac{c_1}{\delta}e^{-(c/\delta)z},$$

where c_1 is another integration constant. Consider now the integral term in the above equation. Evidently, $\int \alpha_s e^{(c/\delta)z}dz \leqslant \int e^{(c/\delta)z}dz = (\delta/c)e^{(c/\delta)z}$, which tends to zero as $z \to -\infty$. Hence, $\int \alpha_s e^{(c/\delta)z}dz$ also tends to zero as $z \to -\infty$. Since $e^{(c/\delta)z} \to 0$ as $z \to -\infty$, the limit of $e^{-(c/\delta)z}\int \alpha_s e^{(c/\delta)z}dz$ can be evaluated by using l'Hôpital's rule

$$\lim_{z\to-\infty}\frac{\int \alpha_s e^{(c/\delta)/z}dz}{e^{(c/\delta)z}} = \lim_{z\to-\infty}\frac{\dfrac{d\alpha_s}{dz}+\dfrac{c}{\delta}\alpha_s}{\dfrac{c}{\delta}} = 0.$$

This then implies that $c_1 = 0$, since $e^{-(c/\delta)z}$ blows up as $z \to -\infty$ and as a result

$$\beta_s = -\frac{6}{\delta}\alpha_s + \frac{6}{\delta}e^{-(c/\delta)z}\left(\frac{1}{\delta}-1\right)\int \alpha_s e^{(c/\delta)z}dz + 6. \quad (25)$$

Therefore, at the back of the front, effectively as $z \to -\infty$ where $\alpha = 0$, we have $\beta = 6$ consistent with the fact that protons are formed by the reaction in a stoichiometric ratio of 6 to 1 with respect to the tetrathionate ions. Notice that in the particular case $\delta = 1$, (25) yields the simple relation $\beta_s(z) + 6\alpha_s(z) = 6$.

The system in (24) can now be written as

$$\frac{d\beta_s}{dz} = v, \quad (26a)$$

$$\frac{d\alpha_s}{dz} = c\left(1-\alpha_s-\frac{\beta_s}{6}\right)-\frac{\delta}{6}v, \quad (26b)$$

$$\frac{dv}{dz} = -\frac{c}{\delta}v - \frac{6}{\delta}Daf(\alpha_s,\beta_s). \quad (26c)$$

We shall examine the (α_s, β_s, v) phase plane where the wavefront is a heteroclinic trajectory connecting the two fixed points (0,6,0) and (1,0,0) associated with the boundary conditions

$$z \to -\infty: \quad \alpha_s \to 0, \beta_s \to 6$$

$$z \to +\infty: \quad \alpha_s \to 1, \beta_s \to 0.$$

Linearization of the dynamical system (26) around the fixed point (0,6,0) yields a Jacobian the spectrum of which is described by three eigenvalues

$$\lambda_1 = -c/\delta, \quad \lambda_2 = (-c-\sqrt{c^2+144\kappa Da})/2,$$

$$\lambda_3 = (-c+\sqrt{c^2+144\kappa Da})/2.$$

Hence, two of the eigenvalues are negative and one eigenvalue is positive. Therefore, the eigenvector associated with the positive eigenvalue must be used in a shooting scheme for the numerical construction of the wavefront. However, no permanent-form traveling wave solutions of Eq. (26) for $c < c_{\min}$ exist, while a unique permanent-form traveling wave exists for each $c > c_{\min}$. To obtain the wavefront with the minimum c, we consider the other fixed point of (26): (1,0,0). Linearization of (26) around this fixed point yields a Jacobian, the spectrum of which is described by

$$\lambda_1 = -c, \quad \lambda_2 = -c/\delta, \quad \lambda_3 = 0.$$

The eigenvectors associated with $\lambda_1 = -c$ and $\lambda_2 = -c/\delta$ are $e_1 = (1,0,0)^t$ and $e_2 = (0,1,-c/\delta)^t$. In the particular case $\delta = 1$, $-c$ becomes an eigenvalue of algebraic and geometric multiplicity 2. For traveling waves of quadratic and cubic autocatalytic systems, Billingham and Needham[39] have proved that for $c = c_{\min}$ the heteroclinic trajectory will approach the second fixed point above the plane spanned by e_1 and e_2. For higher velocities the second fixed point will be approached along e_3 associated with the center manifold and for lower velocities the trajectory is below the plane spanned by e_1, e_2 and will diverge. Notice here that all these propositions from the study by Billingham and Needham can easily be extended to our case—see also the analysis by Billingham[40] of one-dimensional reaction-diffusion waves with degenerate reaction terms. Following these works the condition that the trajectory is always above the plane spanned by e_1, e_2 is simply $v > -c\beta/\delta$, and hence in our shooting scheme we search for the minimum c for which this condition still holds. This method was also employed by Tóth *et al.*[41] to construct the traveling fronts of cubic autocatalytic systems in the presence of an electric field.

We utilize the NAG routine D02EJF (based on backward differentiation and suitable for stiff systems) for the numerical integration of the dynamical system (26) starting from the fixed point (0,6,0). For $c < c_{\min}$, α blows up as $z \to +\infty$ and at the same time β diverges towards large negative values. It is only for $c \geqslant c_{\min}$ that $\alpha \to 1$ and $\beta \to 0$ for large positive z. Figure 2 depicts a minimum speed traveling wavefront for $Da = 0.005$, $\kappa = 1$, and $\delta = 1$ with $c_{\min} = 0.696$. The existence

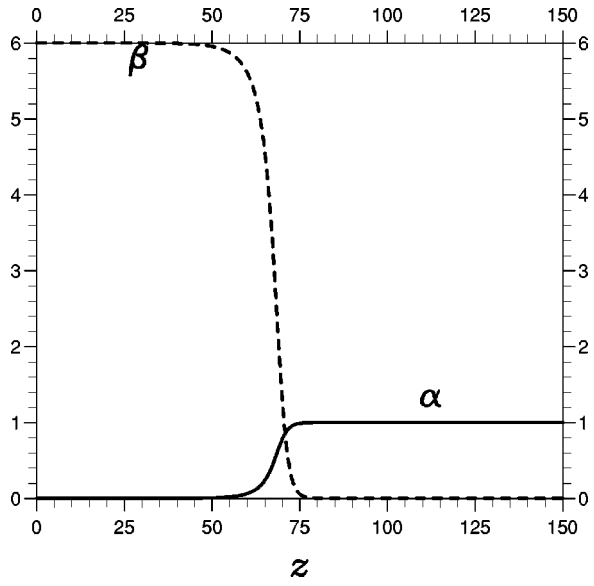

FIG. 2. Stationary traveling wavefront for $Da = 0.005$, $\kappa = 1$, and $\delta = 1$.

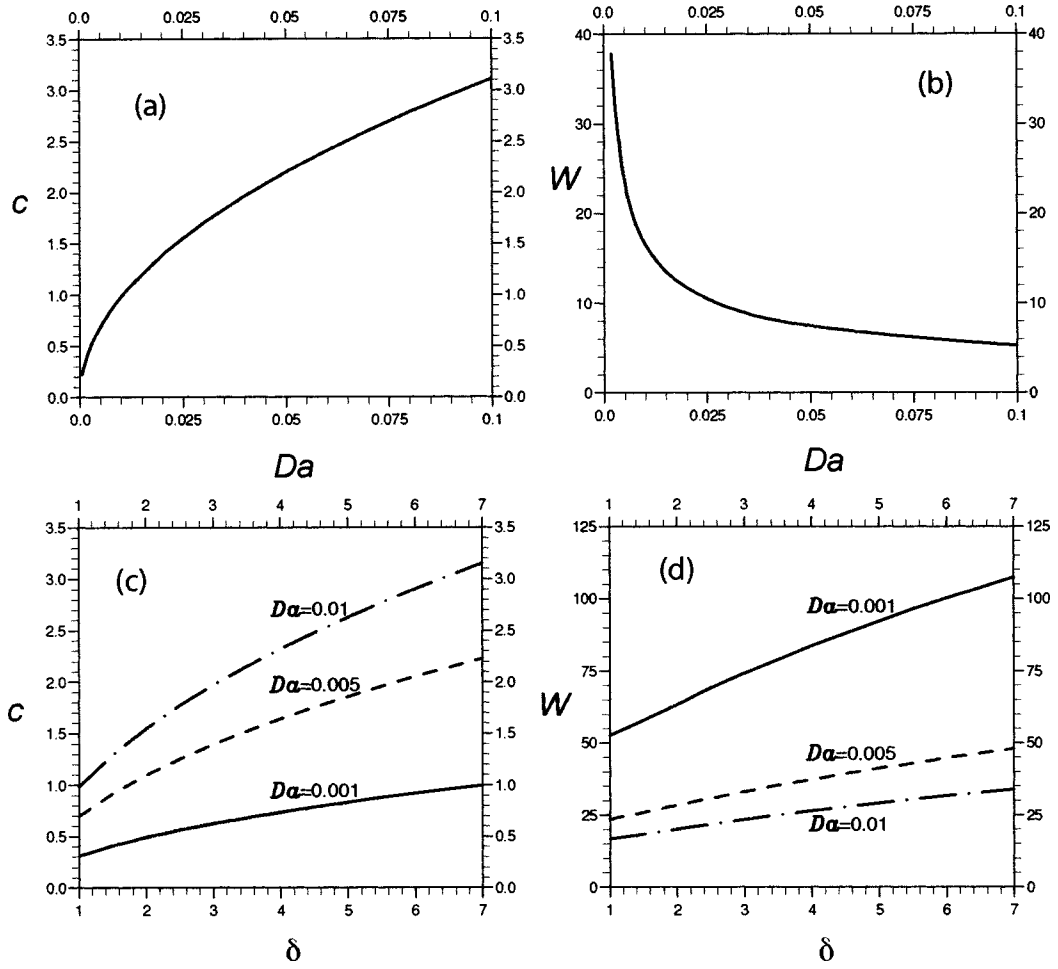

FIG. 3. (a) Dimensionless speed, c, of the reaction-diffusion front as a function of the Damköhler number, Da, for $\delta=1$. The relation $c=9.833\sqrt{Da}$ holds; (b) Dimensionless width, W, of the reaction-diffusion front as a function of Da for $\delta=1$. The width is defined as the domain in which α takes on values in the interval [0.01,0.99]; (c) Dimensionless speed c of the reaction front as a function of δ for different Damköhler numbers; (d) Dimensionless width, W, of the reaction-diffusion front as a function of δ for different Damköhler numbers.

of a minimum speed for the traveling waves raises the question of front selection in the time-dependent reaction-diffusion equations. For this purpose we integrated the reaction-diffusion equations in (20)–(21) with $\underline{u}=\underline{0}$ in time and space as an initial value problem using zero-flux boundary conditions at the ends of a long integration domain. We use a standard Crank–Nicolson-type implicit scheme for solving parabolic equations, with the x derivatives approximated by central differences. Our numerical experiments indicate that the minimum speed wavefront is always approached at large times, provided the initial condition has compact support. A typical initial condition was $\alpha=1$ everywhere and $\beta=0.5$ for the first few grid points at the left boundary of the integration domain while $\beta=0$ in the rest of the domain. In addition, we performed initial value problem computations for the evolution of small amplitude perturbations on the wavefronts of (26) and in all cases sufficiently localized in space perturbations decay to zero for large times. All these computations demonstrate that from the infinite number of traveling solutions for $c\geqslant c_{\min}$, the wavefront with $c=c_{\min}$ is the stable solution. In fact the situation here is similar to Fisher's equation (see for example Ref. 42), where also localized initial conditions always evolve into the traveling wave of minimum speed—see Ref. 43 for a proof of the stability of the minimum speed wavefront of Fisher's equation using renormalization group theory.

Consider now (24a,b). The transformation $z\rightarrow zDa^{-1/2}$ and $c\rightarrow cDa^{1/2}$ scales away Da from these two equations such that the minimum speed is given by $c=\tilde{c}\sqrt{Da}$ with $\tilde{c}=\tilde{c}(\delta)$ the minimum speed for $Da=1$. Our computations show that for $\kappa=1$ and $\delta=1$, $\tilde{c}\simeq 9.833$ such that $c\simeq 9.833\sqrt{Da}$. Figure 3(a) depicts the variation of minimum speed for $\kappa=1$ and $\delta=1$ as a function of Da obtained from the dynamical system in (26). Experimentally, varying Da is easily achieved by varying the initial concentration of tetrathionate ions α_0—see definition (16)—which is known to modify the speed of the wavefront.[28] A fit of the curve in the figure gives $c\sim 9.9\sqrt{Da}$. Figure 3(b) shows the variation of the width, W, of the wavefront (defined as the domain in which α is in the interval [0.01,0.99]) as a function of Da. As expected from the scaling arguments above, W scales as $Da^{-1/2}$, leading to sharper wavefronts traveling at a higher speed when Da is increased. An analogous trend is observed with the traveling waves of the IAA system.[14] Figures 3(c) and 3(d) depict the variation of the speed c and width W as a

function of δ for different Damköhler numbers. Both c and W are increasing functions of δ, while for the same δ increasing Da leads to sharper wavefronts traveling faster. Finally, we point out that Tóth *et al.*[28] have obtained numerically the traveling front solutions of the chlorite–tetrathionate system from initial value calculations of the reaction-diffusion equations and for different values of the diffusivity ratio δ. Their finding $c \sim \alpha_0^{3/2}$ is in excellent agreement with $c \sim \sqrt{Da}$ with Da defined from (16).

IV. LINEAR STABILITY ANALYSIS

A. Eigenvalue problem

We now consider the stability of the wavefront constructed in the previous section with respect to infinitesimal disturbances in the spanwise direction. In the moving frame, $z=x-ct$, the base state of the full set of equations (18)–(21) is simply $\underline{u}=\underline{u}_s=\underline{0}$, $\alpha=\alpha_s(z)$, $\beta=\beta_s(z)$, and $p=p_s(z)$, where

$$\frac{dp_s}{dz}=\gamma_1\alpha_s+\gamma_2\beta_s. \tag{27}$$

Indeed, as $\partial p_s/\partial y=-w_s\equiv 0$, with w the velocity along y, the base state pressure profile is only a function of z and can be easily found by integrating (27) above. Let $\underline{u}=\underline{u}_s+\underline{u}_1$, $\alpha=\alpha_s+\alpha_1$, $\beta=\beta_s+\beta_1$, and $p=p_s+p_1$ with $\underline{u}_1$, α_1, β_1, $p_1 \ll 1$. Linearizing (18)–(23) in the moving frame and utilizing (24), one obtains the evolution equations for the disturbances

$$\frac{\partial p_1}{\partial z}=-u_1+\gamma_1\alpha_1+\gamma_2\beta_1, \tag{28a}$$

$$\frac{\partial p_1}{\partial y}=-w_1, \tag{28b}$$

$$\frac{\partial \alpha_1}{\partial t}-c\frac{\partial \alpha_1}{\partial z}+u_1\frac{d\alpha_s}{dz}=\frac{\partial^2\alpha_1}{\partial z^2}+\frac{\partial^2\alpha_1}{\partial y^2}-Da\left.\frac{\partial f}{\partial \alpha}\right|_{ss}\alpha_1-Da\left.\frac{\partial f}{\partial \beta}\right|_{ss}\beta_1, \tag{28c}$$

$$\frac{\partial \beta_1}{\partial t}-c\frac{\partial \beta_1}{\partial z}+u_1\frac{d\beta_s}{dz}=\delta\frac{\partial^2\beta_1}{\partial z^2}+\delta\frac{\partial^2\beta_1}{\partial y^2}+6Da\left.\frac{\partial f}{\partial \alpha}\right|_{ss}\alpha_1+6Da\left.\frac{\partial f}{\partial \beta}\right|_{ss}\beta_1, \tag{28d}$$

$$\underline{\nabla}\cdot\underline{u}_1=0. \tag{28e}$$

where $|_{ss}$ indicates that the corresponding quantity is evaluated at α_s, β_s.

We now seek particular solutions of (28) in the form of the normal modes

$$[u_1,w_1,p_1,\alpha_1,\beta_1]=[\overline{u}(z),\overline{w}(z),\overline{p}(z),\overline{\alpha}(z),\overline{\beta}(z)]\times e^{\sigma t+iky}+\text{c.c.}, \tag{29}$$

where σ is the growth rate of the infinitesimal disturbances and k their wave number [such solutions are possible since the problem in (28) is homogeneous in both t and y]. Substitution of (29) into (28) then yields

$$\frac{d\overline{p}}{dz}=-\overline{u}+\gamma_1\overline{\alpha}+\gamma_2\overline{\beta}, \tag{30a}$$

$$ik\overline{p}=-\overline{w}, \tag{30b}$$

$$\sigma\overline{\alpha}-c\frac{d\overline{\alpha}}{dz}+\overline{u}\frac{d\alpha_s}{dz}=\frac{d^2\overline{\alpha}}{dz^2}-k^2\overline{\alpha}-Da\left.\frac{\partial f}{\partial \alpha}\right|_{ss}\overline{\alpha}-Da\left.\frac{\partial f}{\partial \beta}\right|_{ss}\overline{\beta}, \tag{30c}$$

$$\sigma\overline{\beta}-c\frac{d\overline{\beta}}{dz}+\overline{u}\frac{d\beta_s}{dz}=\delta\frac{d^2\overline{\beta}}{dz^2}-\delta k^2\overline{\beta}+6Da\left.\frac{\partial f}{\partial \alpha}\right|_{ss}\overline{\alpha}+6Da\left.\frac{\partial f}{\partial \beta}\right|_{ss}\overline{\beta}, \tag{30d}$$

$$\frac{d\overline{u}}{dz}+ik\overline{w}=0. \tag{30e}$$

Differentiating now (30b) and (30e) once with respect to z gives $(d^2\overline{u}/dz^2)+k^2(d\overline{p}/dz)=0$ which, when combined with (30a), results in

$$\left[\frac{d^2}{dz^2}-k^2\right]\overline{u}=-k^2(\gamma_1\overline{\alpha}+\gamma_2\overline{\beta}). \tag{31}$$

Equations (30c,d) and (31) can now be written as

$$\underline{\underline{\mathcal{L}}}\begin{bmatrix}\overline{\alpha}\\ \overline{\beta}\\ \overline{u}\end{bmatrix}=\sigma\begin{bmatrix}1&0&0\\0&1&0\\0&0&0\end{bmatrix}\begin{bmatrix}\overline{\alpha}\\ \overline{\beta}\\ \overline{u}\end{bmatrix}, \tag{32a}$$

where the elements of the matrix/differential operator $\underline{\underline{\mathcal{L}}}$ are given by

$$\mathcal{L}_{11}=\frac{d^2}{dz^2}+c\frac{d}{dz}+\left(-k^2-Da\left.\frac{\partial f}{\partial \alpha}\right|_{ss}\right),$$

$$\mathcal{L}_{12}=-Da\left.\frac{\partial f}{\partial \beta}\right|_{ss};\quad \mathcal{L}_{13}=-\frac{d\alpha_s}{dz};\quad \mathcal{L}_{21}=6Da\left.\frac{\partial f}{\partial \alpha}\right|_{ss},$$

$$\mathcal{L}_{22}=\delta\frac{d^2}{dz^2}+c\frac{d}{dz}+\left(-\delta k^2+6Da\left.\frac{\partial f}{\partial \beta}\right|_{ss}\right),$$

$$\mathcal{L}_{23}=-\frac{d\beta_s}{dz};\quad \mathcal{L}_{31}=-k^2\gamma_1;$$

$$\mathcal{L}_{32}=-k^2\gamma_2,\quad \mathcal{L}_{33}=\frac{d^2}{dz^2}-k^2.$$

The linear stability problem is hence governed by an infinite-domain (generalized) eigenvalue problem. The boundary conditions are

$$\overline{\alpha},\quad \overline{u}\to 0\ \text{ as }\ z\to\pm\infty. \tag{32b}$$

Recall that for $\delta=1$, $\beta_s+6\alpha_s=6$. In this case, (28d) is replaced by

$$\frac{\partial(\beta_1+6\alpha_1)}{\partial t}-c\frac{\partial(\beta_1+6\alpha_1)}{\partial z}$$
$$=\frac{\partial^2(\beta_1+6\alpha_1)}{\partial z^2}+\frac{\partial^2(\beta_1+6\alpha_1)}{\partial y^2},$$

and hence (30d) by

$$\sigma(\overline{\beta}+6\overline{\alpha})-c\frac{d(\overline{\beta}+6\overline{\alpha})}{dz}=\frac{d^2(\overline{\beta}+6\overline{\alpha})}{dz^2}-k^2(\overline{\beta}+6\overline{\alpha}),$$

the general solution of which is $\overline{\beta}(z)+6\overline{\alpha}(z)=A\exp[\frac{1}{2}(-c+\sqrt{c^2+4(k^2+\sigma)})z]+B\exp[\frac{1}{2}(-c-\sqrt{c^2+4(k^2+\sigma)})z]$, where A, B are the integration constants. We can easily show that these integration constants should vanish. Assume for example that $c^2+4(k^2+\sigma)>0$, then as $z\to+\infty$, the exponential term, multiplying A blows up while as $z\to-\infty$ the exponential term multiplying B blows up. Hence, $A=B=0$. Similar arguments apply when $c^2+4(k^2+\sigma)<0$ or when σ is complex. Therefore

$$\overline{\beta}(z)=-6\overline{\alpha}(z), \tag{33}$$

which eliminates $\overline{\beta}(z)$ from the problem all together when $\delta=1$. Equation (30c) then becomes

$$\left[\frac{d^2}{dz^2}+c\frac{d}{dz}-Da\left(\left.\frac{\partial f}{\partial\alpha}\right|_{ss}-6\left.\frac{\partial f}{\partial\beta}\right|_{ss}\right)-\sigma-k^2\right]\overline{\alpha}=\overline{u}\frac{d\alpha_s}{dz}, \tag{34a}$$

and (31) yields

$$\left[\frac{d^2}{dz^2}-k^2\right]\overline{u}=-k^2(\gamma_1-6\gamma_2)\overline{\alpha}.$$

The quantity $\gamma_1-6\gamma_2$ in the right-hand side of the equation above is given by $\gamma_1-6\gamma_2=\hat{\gamma}_1\alpha_0/(\rho_2-\rho_1)-6\hat{\gamma}_2\alpha_0/(\rho_2-\rho_1)$, where the hats denote dimensional quantities. However, $\rho_1=\rho_0+\gamma_1\alpha_0$ and $\rho_2=\rho_0+\gamma_2\beta_0$ which, with $\beta_0=6\alpha_0$, gives $\gamma_1-6\gamma_2\equiv-1$, and the above equation can now be written as

$$\left[\frac{d^2}{dz^2}-k^2\right]\overline{u}=k^2\overline{\alpha}, \tag{34b}$$

such that the linear stability problem for $\delta=1$, now governed by (34a,b), is *independent* of the density coefficients $\gamma_{1,2}$. For $\delta\neq1$, however, $\overline{\beta}\neq6\overline{\alpha}$ and the eigenvalue problem depends on δ and one of the density coefficients—the two coefficients are always related to each other through $\gamma_1-6\gamma_2=-1$. Note that equations (34a,b) have the same form as the evolution equations for the disturbances in the linear stability formulation of the IAA system.[14] This is simply due to the fact that for $\delta=1$ our two-variable model is reduced to a one-variable (fourth-order) model.

The boundary conditions in (32b) imply that we restrict our attention to the discrete spectrum of $\underline{\underline{\mathcal{L}}}$—this spectrum consists of eigenfunctions which decay to zero at the infinities and correspond to disturbances localized around the traveling front. However, since the eigenvalue problem is defined in an infinite domain, we anticipate by analogy with other infinite domain eigenvalue problems (the classical example here is Schrödinger's equation in quantum mechanics) that $\underline{\underline{\mathcal{L}}}$ will also have a continuous essential spectrum which consists of those eigenfunctions with bounded oscillatory behavior at the infinities. This spectrum can be associated with disturbances on the regions sufficiently far from the front, and such disturbances must be expressed in terms of the continuous eigenfunctions which do not decay to zero but approach bounded oscillations at the infinities (but still within the bounds where the infinite-domain formulation is valid). For example, step changes in average concentration which generate effective sources or sinks of α, β. At the same time, as the continuous modes are not localized around the front they represent spatially global modes reflecting the response of the base state away from the front. Preliminary analysis indicates that such modes do exist and indeed the wavefront is unstable to perturbations in the far field—see also the discussion on the stability of the minimum speed wavefront in the previous section. In addition, the continuous eigenfunctions can be related to spatial stability (in contrast to the temporal stability considered here, i.e., we seek the growth rate as a function of the real wave number k) and to classical convective stability theory (see for instance Ref. 44); however, a detailed consideration of the continuous modes as well as the connection with convective stability theory is beyond the scope of the present paper (see Ref. 45 for the construction of the continuous spectrum of the operator governing the stability of free-surface thin-film flows over topography using the Evans function method).

B. Dispersion relations

We solve the eigenvalue problem in (32) numerically by using a second-order central finite-differencing scheme to approximate $\underline{\underline{\mathcal{L}}}$ with its discrete analog. More specifically, if $\underline{U}$, $\underline{A}$, and $\underline{B}$ are the discrete representations of $\overline{u}$, $\overline{\alpha}$, and $\overline{\beta}$, respectively, we invert the discrete representation of the operator $(d^2/dz^2)-k^2$ in (31) to obtain an expression for $\underline{U}$ as a function of $\underline{A}$ and $\underline{B}$ which, when substituted in the discretized version of (30c,d), yields a matrix eigenvalue problem of the form

$$\underline{\underline{M}}\begin{bmatrix}\underline{A}\\ \underline{B}\end{bmatrix}=\sigma\begin{bmatrix}\underline{A}\\ \underline{B}\end{bmatrix}.$$

Thus, we replace a complicated differential eigenvalue problem with a much simpler matrix eigenvalue problem. The eigenvalues and eigenvectors of $\underline{\underline{M}}$ were obtained using the LAPACK solver DGEEVX. A large number of points in the integration domain was necessary for the first few eigenvalues with largest real parts to converge. We tested the accuracy of the numerical scheme by varying the domain size and refining the mesh.

Figure 4(a) depicts the least stable (largest) eigenvalue σ as a function of wave number k for $\kappa=1$, $\delta=1$, and different values of Da. Clearly, the neutral wave number with zero growth rate occurs at zero wave number and at a cutoff wave number, with a band of unstable modes between zero and cutoff. Thus, small amplitude sinusoidal disturbances are linearly unstable (growing) for long wavelengths and stable

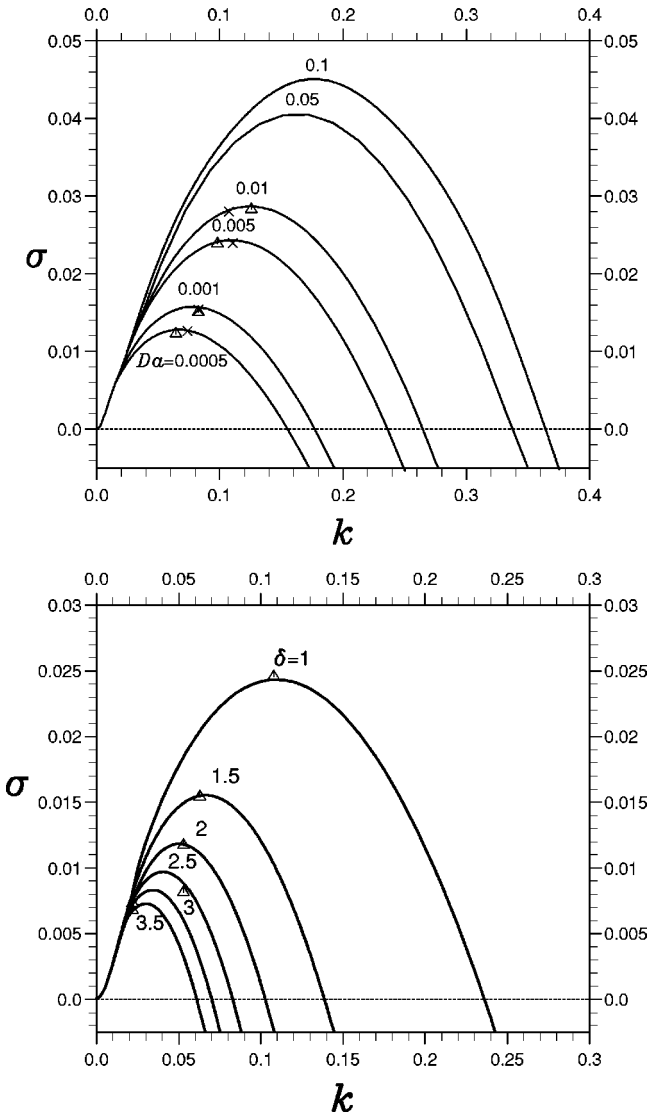

FIG. 4. (a) Dispersion relation for the dimensionless growth rate σ as a function of wave number k for $\delta=1$ and different values of Da. The crosses and triangles are the values obtained from the fully nonlinear system with initial condition a step function or a traveling wavefront, respectively; (b) Dispersion relation for the dimensionless growth rate σ as a function of wave number k for $Da=0.005$ and different values of $\delta(\geqslant 1)$. The values of the density coefficients are $\gamma_1=1.282$ and $\gamma_2=0.38$.

(damping) for short wavelengths. Long-wave disturbances with $k\to 0$ are always unstable and therefore the instability is a long-wave variety.

As we have already demonstrated, the hypothesis of equal diffusivities reduces the two-variable CT model to a one-variable (fourth-order) model, allowing for an interesting comparison with the one-variable (cubic) IAA system. We can then establish to what extend the stability properties of chemical fronts and the resulting nonlinear dynamics are kinetics/model dependent. Evidently, the dispersion relation for the CT and IAA systems is similar: in both cases, long wavelengths are unstable and short wavelengths stable, while the band of unstable wave numbers increases by increasing the Damköhler number, i.e., a more hydrodynamically unstable situation. As already discussed for the IAA fronts,[14] increasing Da leads to faster and sharper fronts which counterbalance the stabilizing effect of diffusion.

Figure 4(b) shows σ as a function of k for a typical value of the Damköhler number, $Da=0.005$, $\kappa=1$, and different values of $\delta(\geqslant 1)$. Following Ref. 46, the density coefficients are taken to be $\gamma_1=1.282$ and $\gamma_2=0.38$. Clearly, increasing δ stabilizes the front. This is due to the fact that increasing δ leads to faster wavefronts with larger widths [see Figs. 3(c) and 3(d)]. If the front has a higher velocity, the fingers cannot develop as easily since they are entrained by the front, resulting in a more stable situation. At the same time, larger widths weaken the density gradient and hence diminish the overall destabilizing force.

Interestingly enough, the growth rate curves for $\delta\neq 1$ remain qualitatively similar to those for $\delta=1$, i.e., there is always a band of unstable modes from $k=0$ up to a critical wave number above which the growth rate is negative. The main features of the fingering instability are thus *independent* of the value of the diffusivity ratio which brings in only quantitative changes of the growth rate: varying δ from 1 to 3 leads to a maximum growth rate and a maximum growing wave number that are both reduced by a factor of 3.

The region $k\to 0$ deserves special attention. We can show that $\sigma=0$ for $k=0$. For simplicity, let us assume $\delta=1$. With $k=0$ in (34b), we obtain $\overline{u}_{zz}=0$ and since $\overline{u}\to 0$ as $z\to\pm\infty$, we have $\overline{u}=0$. With $\overline{u}=k=\sigma=0$, (34a) gives

$$\frac{d^2\overline{\alpha}}{dz^2}+c\frac{d\overline{\alpha}}{dz}-Da\left(\left.\frac{\partial f}{\partial\alpha}\right|_{ss}-6\left.\frac{\partial f}{\partial\beta}\right|_{ss}\right)\overline{\alpha}=0. \tag{35}$$

Differentiating now Eq. (24a) once with respect to z and using $\beta_s+6\alpha_s=6$, gives

$$\frac{d^3\alpha_s}{dz^3}+c\frac{d^2\alpha_s}{dz^2}-Da\left(\left.\frac{\partial f}{\partial\alpha}\right|_{ss}-6\left.\frac{\partial f}{\partial\beta}\right|_{ss}\right)\frac{d\alpha_s}{dz}=0 \tag{36}$$

which when compared with (35) shows that $\overline{\alpha}=d\alpha_s/dz$ within an arbitrary multiplicative constant (notice that the derivative of α_s with respect to z has a maximum at $\alpha_s=1/2$, which is thus the point mostly influenced by the disturbances). Hence, the operator $\underline{\underline{\mathcal{L}}}$ has a one-dimensional null space spanned by the eigenfunction $[d\alpha_s/dz,0]^t$. This eigenfunction is associated with the translational invariance of the system in the z-direction: since Eq. (24) is invariant to a shift in z, if α_s is a solution, so must be its translate $\alpha_s(z-\hat{c}(t))$, and hence there is a family of possible solutions generated by the translation. If one perturbs the front slightly, that is, $\hat{c}(t)\ll 1$, then $\alpha_s(z-\hat{c}(t))\sim\alpha_s(z)-\hat{c}(t)\alpha_{sz}(z)$, where $\hat{c}(t)\alpha_{sz}(z)$ is the perturbation due to translation. When this expression is now substituted into (24), and after linearizing for $\hat{c}\ll 1$, and differentiating the resulting equation once with respect to z, one obtains (36): the translational symmetry manifests itself as a null eigenfunction.

This eigenfunction would be the key component in the derivation of a nonlinear evolution equation for the location of the developed fingers in the weakly nonlinear regime of the instability. We have already shown that the linearized operator of the nonlinear system yields a spectrum with a zero eigenvalue. Moreover, our computations reveal that the zero eigenvalue is well isolated from the higher order nega-

tive eigenvalues (or eigenvalues with negative real parts). Such nonlinear systems exhibit a unique nonlinear dynamics near the equilibrium points: any sufficiently rich initial disturbance will excite all the modes in the spectrum, however, for small but finite-amplitude disturbances, the modes associated with the negative eigenvalues will relax very rapidly and the system trajectory will approach exponentially fast to an invariant manifold of the same dimension as the number of zero eigenvalues. Hence, instead of modeling the entire infinite-dimensional nonlinear dynamics, one needs only to decipher the low-dimensional and slow nonlinear dynamics on the invariant manifold. One could then use techniques from dynamical systems theory, namely center manifold projection, to obtain the evolution of the fingers in the weakly nonlinear stage of the instability. Such analysis would be effectively analogous to Kuramoto's multiple scale analysis for the dynamics of slowly varying wavefronts (kinks or pulses).[34] Typically, a Kuramoto–Sivashinsky-type equation for the nonlinear evolution of disturbances from a large-amplitude pattern is derived—see also Ref. 47 for the derivation of this equation for viscous shock waves in free-surface thin-film flows using center manifold projection. Although the derivation of this evolution equation for the chlorite–tetrathionate system is beyond the scope of the present study, we anticipate that by analogy with Kuramoto's approach, the equation will have a second spatial derivative, accounting for energy production and a fourth spatial derivative, accounting for energy dissipation. Hence, long waves are unstable and the growth rate in the region of $k \to 0$ is analogous to k^2. This observation is consistent with our numerical solution of the eigenvalue problem in (32), which shows that indeed $\sigma \sim k^2$ in the region of small wave numbers. This behavior can also be obtained from simple symmetry considerations: the translational invariance of the traveling wave solution in the streamwise direction implies that $\sigma = 0$ for $k = 0$, while space reflection invariance in the y direction implies that σ is invariant under the transformation $k \to -k$, or alternatively that the evolution equation for the developed fingers is symmetric under $y \to -y$.

Therefore, the situation here is quite different from the problem considered by Tan and Homsy,[48,49] where the growth rate, for small times, is a linear function of wave number in the region of small wave numbers. In fact, Tan and Homsy[48] obtain analytically the growth rate as a function of wave number for viscous miscible fingering in a Hele–Shaw cell. Their analysis is based on the assumption of an initially sharp interface between the two fluids, effectively a step function for the concentration of the solvent—see also the discussion in Ref. 14 for the dispersion relation at $t = 0$ in pure density fingering in the absence of chemical reactions. The assumption that the system evolves in a quasisteady manner makes the base state translationally invariant, and hence $\sigma = 0$ for $k = 0$. (Notice, however, that strictly speaking, diffusion is a nonstationary process; in fact, the base state is self-similar in time and hence although the equation itself is translationally invariant, its solution is not.) Space reflection symmetry would then imply that σ is invariant under the transformation $k \to -k$ as we discussed above; however, the growth rate now scales as $\sigma \sim |k|$ in the neighborhood of small k and not as k^2. This is due to the discontinuity of the base state at $t = 0$ (Tan and Homsy assumed a step function for the concentration at $t = 0$), which manifests itself as a discontinuity for the derivative of σ at $k = 0$. In fact, a simple analysis of the solution obtained by Tan and Homsy shows that the perturbations for the concentration, velocity, and pressure are continuous at $k = 0$ but their derivatives are discontinuous in this limit. It would then seem reasonable to conclude that the growth rate is no longer a linear function of k at later times, when diffusion smoothes out the initial discontinuity of the concentration profile; however, computations for the growth rate in the region of $k = 0$ have not been reported.

The fundamental difference therefore between the system considered here, as well as the IAA system and pure miscible fingering, is that the base state in the presence of chemical reaction is a traveling front in a moving frame and this front results from competition between diffusion and reaction. In the absence of chemical reactions, however, there will be no stationary front in a moving frame, as diffusion is simply a nonstationary process. In fact, if the quasisteady assumption is abandoned one expects that the growth rate of infinitesimal disturbances will no longer be exponential in time. As a result, the presence of chemical reactions has a profound impact on the behavior of the dispersion relation for $k \to 0$ with the growth in this region due to the translational invariance of the reaction-diffusion front in the streamwise direction. For the same reason, the dispersion relation in Ref. 41 for the lateral instability of cubic autocatalytic fronts in the presence of electric field is quadratic with respect to k in the region of small k. This is also the case for the chemoconvection process analyzed in Ref. 50.

Finally, Fig. 5 shows the growth rate $\sigma_{\max}$ and the most unstable wave number $k_{\max}$ as a function of Damköhler number for $\delta = 1$. As Da decreases, the maximum growth rate decreases and eventually tends to zero as $Da \to 0$, since there is practically no chemical reaction in this limit and hence there is no density difference between the two phases. Interestingly enough, the maximum growing wave number is a weak function of Da for large Da.

C. Comparison to experiments

Let us now compare our theoretical results with very recent experimental data.[46] It is known that protons diffuse intrinsically faster than the other species in the CT system. Let us take $\delta = 3$—see for example Ref. 29. The main dimensionless group in our analysis is the Damköhler number. Using its definition in (16) and the characteristic value for the hydrodynamic velocity, $U = \Delta\rho g a^2/12\nu$, we get

$$Da = \frac{144 D_\alpha \nu^2 q \alpha_0^3}{(\Delta\rho g a^2)^2}.$$

Unfortunately, it is not straightforward to use this definition to obtain Da due to the uncertainty on the kinetic parameter[51] q and on the diffusion coefficient D_α.[29,30] Instead, we choose to compute Da using our numerical result in Fig. 3(c), $Da \sim (c/20)^2$ for $\delta = 3$. As the dimensionless speed of the stable wavefront is $c = v/U$, we obtain

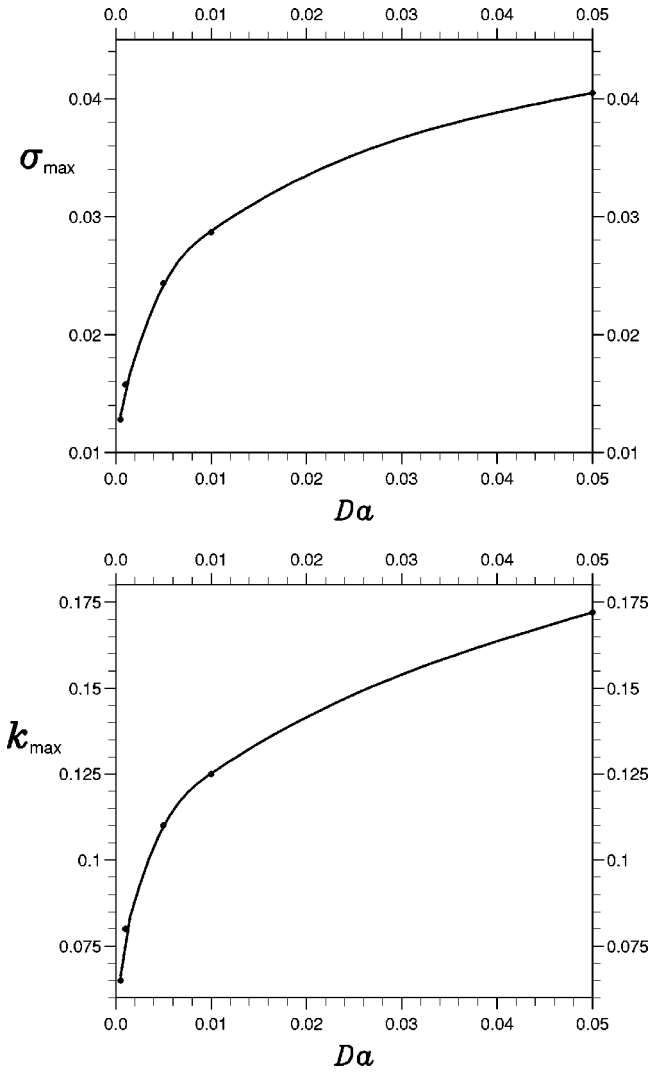

FIG. 5. (a) Dimensionless maximum growth rate in Fig. 4(a) as a function of *Da*. (b) Dimensionless maximum growing wave number in Fig. 4(a) as a function of *Da*.

$$Da=\left(\frac{v}{20U}\right)^2=\left(\frac{12\nu v}{20\Delta\rho g a^2}\right)^2. \tag{37}$$

This definition allows us to compare experimental and theoretical results provided three variables are known, i.e., the gap width a, the density ratio $\Delta\rho$, and the velocity of the stable chemical front v. A typical set of experimental parameters is $a=0.821$ mm, $\Delta\rho=3.1\times10^{-4}$,[46] $v=0.12$ mm/s for $\alpha_0=5.0\times10^{-3}$ M,[28] while we use $g=9.8\times10^3$ mm/s^2 and take $\nu=0.99$ mm^2/s, the kinematic viscosity of water as we are dealing with diluted aqueous solutions. These parameters give us $Da=0.0012$. Figure 3(c) then indicates that the traveling reaction-diffusion front has a velocity $c\simeq0.6$, which corresponds to a dimensional velocity $v\simeq0.10$ mm/s. For $Da=0.0012$ our computations show that the most unstable wave number is $k_{\max}\simeq0.05$. To convert this to a dimensional quantity, we need the diffusivity D_α in the definition of the hydrodynamic length scale in (8). Following Ref. 46, $D_\alpha\simeq1.2\times10^{-2}$ mm^2/s, which with $U\simeq0.17$ mm/s gives a dimensional maximum growing wave number of $\simeq0.7$ mm^{-1} of the same order of magnitude as the experimental value of 1.7 mm^{-1}.[46] Let us nevertheless be cautious as, in the recently reported experimental data, heat effects due to the exothermicity of the reaction were present. Such heat effects have a profound influence on the density ratio $\Delta\rho$, which in turn affects *Da* and the density coefficients $\gamma_{1,2}$ and therefore the maximum growing wave number. Hence, we refrain from a detailed comparison with our theory and at this stage comparisons with experiments can only be qualitative. Note also that combining definitions (16) and (37) of the Damköhler number allows to express the dimensional kinetic constant q simply as

$$q=\frac{v^2}{400D_\alpha\alpha_0^3},$$

which for $v=0.12$ mm/s, $\alpha_0=5.0\times10^{-3}$ M,[28] and $D_\alpha\simeq1.2\times10^{-2}$ mm^2/s gives $q=2.4\times10^4$ M^{-3} s^{-1}.

The experiments are also performed for various angles of the Hele–Shaw cell with respect to the vertical direction.[46] If θ denotes the angle between the Hele–Shaw cell and the vertical direction, the gravitational field is now $g\cos\theta$. When $\cos\theta=0$, the cell is horizontal and no instability takes place. Thus, we anticipate that the maximum growth rate will decrease as $\cos\theta$ decreases from 1 to 0. To compare with the results in Ref. 46 discussed for the special case $\delta=1$, here we define the Damköhler number as $Da=1/\xi^2\cos^2\theta$, where $\xi=10\Delta\rho g a^2/12\nu v$. Using our numerical results for the maximum growth rate in Fig. 5, we can easily obtain $\sigma_{\max}$ and $k_{\max}$ as a function of $\cos\theta=1/\xi\sqrt{Da}$, provided of course we choose a value of the gap width a to compute ξ. The result for $a=1.04$ mm and $\Delta\rho=3.8\times10^{-4}$ is $k^d_{\max}\sim(\cos\theta)^{0.62}$ and $\sigma^d_{\max}\sim(\cos\theta)^{1.5}$, where $k^d_{\max}$ and $\sigma^d_{\max}$ are dimensional quantities. Again, changing a, $\Delta\rho$, γ_1, γ_2, D_α, and δ will change these exponents, which points to the need for precise measurements of all these parameters. We note also that Darcy's law used here is strictly a two-dimensional model and does not take hydrostatic pressure along the gap-width into account, which might be important in tilted configurations, especially when the angle θ departs severely from 0°.

V. NONLINEAR SIMULATIONS

To validate the linear stability analysis of the previous section, and to get insight into the long term nonlinear dynamics of the developed fingers, we consider the full nonlinear equations (18)–(22) with $\delta=1$. Recall that in this case $\beta(z)=6-6\alpha(z)$, and hence β can be eliminated from the equations to give

$$\underline{\nabla}\cdot\underline{u}=0, \tag{38a}$$

$$\underline{\nabla}p=-\underline{u}+[(\gamma_1-6\gamma_2)\alpha+6\gamma_2]\underline{i}_x, \tag{38b}$$

$$\frac{\partial\alpha}{\partial t}+\underline{u}\cdot\underline{\nabla}\alpha=\nabla^2\alpha-36Da\,\alpha(1-\alpha)^2(\kappa+7\alpha). \tag{38c}$$

To integrate this set of equations numerically, we introduce the stream function ψ such that $u=\partial\psi/\partial y$ and $w=-\partial\psi/\partial x$ with $\underline{u}=(u,w)$ the velocity field. Taking the curl of the evolution equation for the pressure perturbation (38b) and recalling that $\gamma_1-6\gamma_2=-1$, gives

$$\psi_{xx}+\psi_{yy}=-\alpha_y, \tag{39a}$$

$$\alpha_t+\alpha_x\psi_y-\alpha_y\psi_x=\alpha_{xx}+\alpha_{yy}-36Da\,\alpha(1-\alpha)^2\times(\kappa+7\alpha). \tag{39b}$$

We numerically solve Eqs. (39a,b) using a pseudospectral method[49,52] on a two-dimensional domain of dimensionless width L_y' and length L_x'. We note that the dimensionless width is simply $L_y'=L_y/L_h=L_yU/D_\alpha=\Delta\rho g a^2 L_y/12\nu$, which is the equivalent of a Rayleigh number, *Ra*. If we define the aspect ratio A as $A=L_x/L_y$, we obtain $L_x'=ARa$.

Our numerical scheme is essentially based on Fourier expansions for the stream function ψ and concentration α, and hence periodic boundary conditions are imposed in both the transverse and streamwise directions. We derive a set of ordinary differential equations (ODE) for the evolution of the time-dependent coefficients of the Fourier expansions. These ODEs are solved numerically using a second-order Adams–Bashforth scheme. There is no problem in the use of periodic boundary conditions in the transverse direction. To deal with periodicity in the x direction, we start with $\alpha=0$ at the top ($x=0$) of the cell and switch to $\alpha=1$ at $x=0.05L_x'$. The downward traveling front has heavier product on top (corresponding to $\alpha=0$), invading the lighter reactants ($\alpha=1$) below, and hence it is buoyantly unstable. The reverse switch from $\alpha=1$ to 0 applied at the bottom $x=0.95L_x'$ on the contrary corresponds to a heavier solution invading upwards the lighter reactants which is a buoyantly stable situation. Two different initial conditions were used in all our numerical simulations: a step function or the planar wavefront obtained from our shooting scheme in Sec. III. Appropriately smoothed random white noise of 0.2% maximum amplitude is applied at the front. Figure 6 shows a typical nonlinear evolution of the upper hydrodynamically unstable front for $Da=0.005$, $\kappa=1$, and $\delta=1$ using as an initial condition a step function (in all cases, the nonlinear dynamics for $\delta=1$ is qualitatively similar to that for $\delta\neq1$). The observed pattern is very similar to what is observed in the experiments.[46] To compare our nonlinear simulations to the linear stability analysis of Sec. IV, we measure the maximum growth rate and most unstable wavelength. The growth rate is obtained by fitting an exponential to the evolution of the length of the fingers as a function of time for small times.[53] To obtain the wavelength of the developed fingers we take the power spectrum of the front at early times. The dimensionless wavelength of the developed fingers is 0.098 ± 0.006, in excellent agreement with the $\simeq0.1$ value predicted by the linear stability theory of the previous section. Figure 4 compares the linear stability analysis with the fully nonlinear simulations and in all cases the agreement is very good. The results are roughly the same whether the initial condition is a step function or the traveling wave solution.

At later times, some of the fingers merge, leading to an overall coarsening of the fingering pattern (see Figs. 6 and 7). In narrower systems (Fig. 7) the front evolves ultimately to one single finger of constant mixing zone (defined as the distance between the most advanced point of the front beyond which $\alpha>0.99$ and the back of the front behind which $\alpha>0.01$). This fingered front travels at a constant speed higher than the minimum speed c of the stable reaction-diffusion front. This increased speed results from entrainment of the flow due to the presence of convection rolls. As an example, for $Da=0.001$ (Fig. 7), the stable planar front travels at a speed $c=0.311$, while the single final finger of Fig. 7(d), reached after all fingers have merged, travels at a constant speed equal to 0.582. Increasing the Damköhler number favors the chemical component of the dynamics over the hydrodynamics. Hence, as reaction-diffusion processes favor planar fronts, increasing *Da* leads to less developed fingers characterized by a smaller mixing zone as can be seen

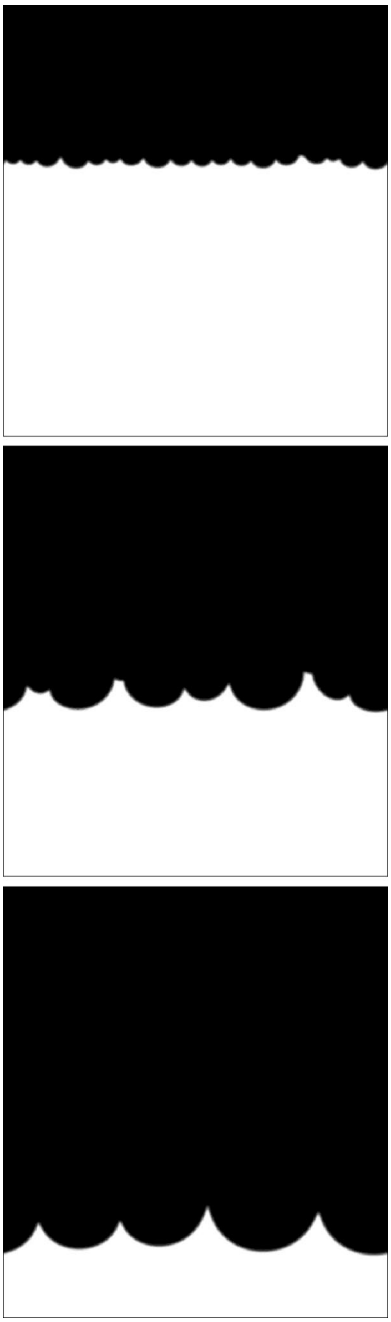

FIG. 6. Density plot of the fingering instability at various times for $Da=0.005$, $\kappa=1$, $Ra=1024$, and $\delta=1$. The initial condition is a step function. The system is shown from top to bottom at three successive times $t=600$, 900, and 1200.

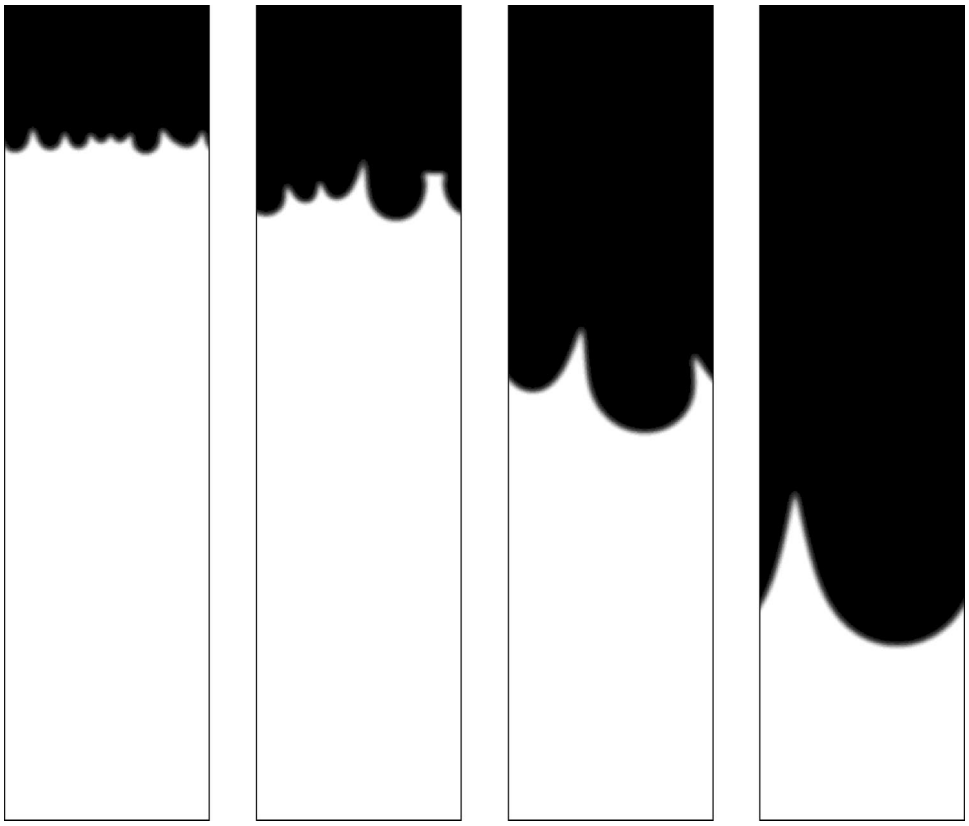

FIG. 7. Density plot of the fingering instability at various times for $Da=0.001$, $\kappa=1$, $Ra=512$, and $\delta=1$. The initial condition is a step function. The system is shown from left to right at four successive times $t=900$, 1200, 2100, and 3000.

when comparing Figs. 6(c) and 7(b). In addition, the presence of chemical reactions changes the up/down symmetry observed in pure density fingering[53,54] because of the front movement direction.

VI. DISCUSSION

We have examined in detail the Rayleigh–Taylor instability of reaction-diffusion fronts for the CT system. We performed a linear stability analysis of the minimum speed wavefront with respect to infinitesimal disturbances in the spanwise direction and for different values of the Damköhler number. Our analysis revealed the existence of a preferred wavelength for the instability. Both maximum growing wave number and maximum growth rate were found to be in excellent agreement with time-dependent simulations of the fully nonlinear system. The agreement with experimental data is also good.

Unlike the IAA system studied before, where the base state can be obtained analytically in certain limits and its speed is then uniquely defined, for the CT reaction the wavefront has to be obtained numerically and there is an infinite number of possible wavefronts for a speed larger than a minimum value. Having established, however, that the minimum speed wavefront is always the one selected by the CT system (provided that any disturbances are sufficiently localized around the front), we find that for both systems the dimensionless speed is proportional to $Da^{1/2}$, while the width scales as $Da^{-1/2}$. In addition, for $\delta=1$, the CT reaction scheme reduces to a single variable model like the IAA system. It is not surprising then that the dispersion relation for the CT and IAA systems is similar. For example, long wavelengths are unstable and short wavelengths stable for both cases, while the band of unstable wave numbers shrinks by decreasing the Damköhler number, resulting in a more stable situation. Comparison between the dispersion curves for the CT system (Fig. 4) and for the IAA system (Fig. 2 of Ref. 14) shows that the most unstable growth rates and the band of unstable wave numbers are in the same range in both systems for values of parameters representative of the respective experimental conditions. The values of *Da* numbers relevant to experiments are much smaller for the CT system than for the IAA system, but this is just related to the fact that the chemical time scale is defined arbitrarily using the kinetics of the chemical reaction at hand. The *Da* number range will thus strongly depend on the chemical reaction studied. Nevertheless, the wave number of the most unstable mode is of the same order of magnitude in both CT and IAA systems, as it depends on parameters such as gap width a, density difference $\Delta\rho$, diffusion coefficient D_α, and velocity v of the stable front, which are in the same range in both systems. Thus, it seems that both CT and IAA systems behave in a similar fashion with respect to the buoyancy-driven Rayleigh–Taylor instability. The fact that the CT front travels downwards in the gravity field while the IAA front moves upwards does not matter as pure density fingering is intrinsically symmetric with regards to the up/down symmetry. The effect of chemistry is then to introduce a propagation direction which breaks this up- and down-symmetric density fingering.

Assuming $\delta\neq 1$ complicates our analysis as β cannot be eliminated. We then have an additional variable in our linear stability and time-dependent computations. In addition, the

density coefficients, γ_1 and γ_2 also cannot be eliminated from the linearized equations for the disturbances (see the discussion in Sec. III).

The dispersion curves for $\delta > 1$ are qualitatively similar to those obtained for $\delta = 1$, i.e., there is always a band of unstable modes extending from zero wave number up to a critical wave number above which the system is always linearly stable. Hence, the main features of the fingering instability do not depend on the value of the diffusivity ratio—the maximum growing wave number for example is simply reduced by a factor of 3 when δ increases from 1 to 3.

The analysis presented here was based on a number of assumptions. First, we used Darcy's law to describe the fluid velocity in a Hele–Shaw cell. As Darcy's law is a good description for Hele–Shaw flows only for gap widths $a \to 0$, it is probably not a suitable hydrodynamic description of the flow field in the larger cells used in the experiments. Martin and co-workers have recently examined the region of applicability of Darcy's law in the description of Rayleigh–Taylor instability of fronts between miscible fluids in Hele–Shaw cells.[55] For the IAA system, in particular, they have shown that Darcy's law should be replaced by two-dimensional Navier–Stokes–Darcy and eventually three-dimensional Navier–Stokes equations for better quantitative agreement with the experimental dispersion relation curves when the gap width is increased.[15] An analogous study for the CT system would be of particular interest.

Moreover, the quantitative comparison between the present theory and experiments relies heavily on accurate values of the gap width a, the density difference $\Delta\rho$, the diffusivity ratio δ, the diffusion coefficient D_α, and the kinetic parameters. For the time being several of these parameters are not known with great accuracy (see for instance Refs. 29 and 30 regarding D_α) and hence we cannot directly compare the theory presented here and experiments. Notice that in the recently reported experiments by Horváth *et al.*,[46] heat effects due to the exothermicity of the reaction were present. These effects will be analyzed in detail in a future study.[56]

We close with a discussion on the diffusivity ratio δ. For normal aqueous solutions $\delta = 3$ as the protons diffuse probably at least three times faster than the tetrathionate ions.[30] However, the diffusivity ratio depends crucially on the amount of inert salt present in the system. By adding some inert salt, one can in fact increase the apparent diffusion rate of the hydrogen ions. When there is an excess of ions, the hydrogen ions are free to diffuse, and in that case the diffusivity ratio can be as high as 7. In the absence of excess salt in hydrogel, the diffusivity ratio is between 1 and 2. The case $\delta < 1$ would also be of interest. Such a situation can be experimentally achieved by binding the protons to a high molecular weight molecule of reduced mobility carrying carboxylic groups.[30,31] The inhibitor species (tetrathionate ions) will then diffuse apparently quicker than the activator species (protons), allowing for a diffusive destabilization of the front. Such an instability gives rise to a purely diffusive (i.e., convectionless) cellular deformation of the front and has been studied both experimentally and theoretically for the CT system. Performing analogous experiments in vertically oriented Hele–Shaw cells with downwards buoyantly unstable CT fronts might lead to a competition between purely hydrodynamic and diffusive instabilities which could give rise to new interesting spatiotemporal dynamics.

ACKNOWLEDGMENTS

The authors wish to thank A. Tóth and D. Horváth for fruitful discussions and for sharing their experimental results with us prior to publication. We acknowledge financial support from the ESF Research Program REACTOR. J.Y. is grateful to the University of Leeds for financial support and for an ORS award. A.D.O. is a postdoctoral fellow from the Université Libre de Bruxelles. S.K. thanks Professor Eugene Demekhin from the Chemical Engineering Dept. of the University of Notre Dame for numerous stimulating discussions on spectral analysis of linear operators and infinite-domain eigenvalue problems. A.D.W. is Chercheur Qualifié du FNRS (Belgium) and acknowledges financial support from the FRFC (Belgium), Prodex [Contract No. 14556/00/NL/SFe(IC)] and ESA (Contract No. 15196/01/NL/SH).

[1] S. Chandrasekhar, *Hydrodynamic and Hydromagnetic Stability* (Clarendon, Oxford, 1961).
[2] I. R. Epstein and J. A. Pojman, *An Introduction to Nonlinear Chemical Dynamics* (Oxford University Press, Oxford, 1998).
[3] S. K. Scott, *Chemical Chaos* (Oxford University Press, Oxford, 1991).
[4] J. D. Murray, *Mathematical Biology* (Springer, Berlin, 1989).
[5] J. A. Pojman, I. R. Epstein, T. J. McManus, and K. Showalter, J. Phys. Chem. **95**, 1299 (1991).
[6] J. Masere, D. A. Vasquez, B. F. Edwards, J. W. Wilder, and K. Showalter, J. Phys. Chem. **98**, 6505 (1994).
[7] B. F. Edwards, J. W. Wilder, and K. Showalter, Phys. Rev. A **43**, 749 (1991).
[8] D. A. Vasquez, J. W. Wilder, and B. F. Edwards, J. Chem. Phys. **98**, 2138 (1993).
[9] J. Huang, D. A. Vasquez, B. F. Edwards, and P. Kolodner, Phys. Rev. E **48**, 4378 (1993).
[10] J. Zhu, Phys. Fluids **10**, 775 (1998).
[11] J. Huang and B. F. Edwards, Phys. Rev. E **54**, 2620 (1996).
[12] M. R. Carey, S. W. Morris, and P. Kolodner, Phys. Rev. E **53**, 6012 (1996).
[13] M. Böckmann and S. C. Müller, Phys. Rev. Lett. **85**, 2506 (2000).
[14] A. De Wit, Phys. Rev. Lett. **87**, 054502 (2001).
[15] J. Martin, N. Rakotomalala, D. Salin, M. Böckmann, and S. C. Müller, J. Phys. IV **11**, 99 (2001).
[16] A. Hanna, A. Saul, and K. Showalter, J. Am. Chem. Soc. **104**, 3838 (1982).
[17] A. Saul and K. Showalter, in *Oscillations and Traveling Waves in Chemical Systems*, edited by R. J. Field and M. Burger (Wiley, New York, 1985).
[18] J. H. Merkin and H. Sevcikova, Phys. Chem. Chem. Phys. **1**, 91 (1999).
[19] I. Nagypal, G. Bazsa, and I. R. Epstein, J. Am. Chem. Soc. **108**, 3635 (1986).
[20] S. Su, R. L. Armstrong, M. Menzinger, A. Cross, and C. Lemaire, J. Chem. Phys. **98**, 7295 (1993).
[21] C. R. Chinake and R. H. Simoyi, J. Phys. Chem. **98**, 4012 (1994).
[22] J. A. Pojman, V. M. Ilyashenko, and A. M. Khan, J. Chem. Soc., Faraday Trans. **92**, 2825 (1996).
[23] D. Zhang, W. R. Peltier, and R. L. Armstrong, J. Chem. Phys. **103**, 4069 (1995).
[24] B. McCaughey, J. A. Pojman, C. Simmons, and V. A. Volpert, Chaos **8**, 520 (1998).
[25] M. Garbey, A. Taïk, and V. A. Volpert, Q. Appl. Math. **56**, 1 (1998).
[26] I. Nagypál and I. R. Epstein, J. Phys. Chem. **90**, 6285 (1986).
[27] L. Szirovica, I. Nagypál, and E. Boga, J. Am. Chem. Soc. **111**, 2842 (1989).

[28] A. Tóth, D. Horváth, and A. Siska, J. Chem. Soc., Faraday Trans. **93**, 73 (1997).
[29] J. Boissonade, E. Dulos, F. Gauffre, M. N. Kuperman, and P. De Kepper, Faraday Discuss. **120**, 353 (2001).
[30] M. Fuentes, M. N. Kuperman, and P. De Kepper, J. Phys. Chem. A **105**, 6769 (2001).
[31] A. Tóth, I. Lagzi, and D. Horváth, J. Phys. Chem. **100**, 14837 (1996).
[32] A. Tóth, B. Veisz, and D. Horváth, J. Phys. Chem. A **102**, 5157 (1998).
[33] D. Horváth and A. Tóth, J. Chem. Phys. **108**, 1447 (1998).
[34] Y. Kuramoto, *Chemical Oscillations, Waves and Turbulence* (Springer, Berlin, 1984).
[35] D. Horváth, V. Petrov, S. K. Scott, and K. Showalter, J. Chem. Phys. **98**, 6332 (1993).
[36] D. Horváth and K. Showalter, J. Chem. Phys. **102**, 2471 (1995).
[37] G. M. Homsy, Annu. Rev. Fluid Mech. **19**, 271 (1987).
[38] E. Holzbecher, *Modeling Density-Driven Flow in Porous Media* (Springer, Berlin, 1998).
[39] J. Billingham and D. J. Needham, Philos. Trans. R. Soc. London, Ser. A **334**, 1 (1991).
[40] J. Billingham, Dyn. Stab. Syst. **V15-1**, 23 (2000).
[41] A. Tóth, D. Horváth, and W. van Saarlos, J. Chem. Phys. **111**, 10964 (1999).
[42] J. Gazdag and J. Canosa, J. Appl. Probab. **11**, 445 (1974).
[43] G. C. Paquette, L. Y. Chen, N. Goldnfeld, and Y. Oono, Phys. Rev. Lett. **72**, 76 (1994).
[44] P. Huerre in *Hydrodynamics and Nonlinear Instabilities*, edited by C. Godrèche and P. Manneville (Cambridge University Press, Cambridge, 1998).
[45] S. Kalliadasis and G. M. Homsy, J. Fluid Mech. **448**, 387 (2001).
[46] D. Horváth, T. Bánsági, Jr., and A. Tóth, J. Chem. Phys **117**, 4399 (2002) and personal communication.
[47] S. Kalliadasis, J. Fluid Mech. **413**, 355 (2000).
[48] C. T. Tan and G. M. Homsy, Phys. Fluids **29**, 3549 (1986).
[49] C. T. Tan and G. M. Homsy, Phys. Fluids **31**, 1330 (1988).
[50] M. A. Bees, A. J. Pons, P. G. Sorensen, and F. Sagués, J. Chem. Phys. **114**, 1932 (2001).
[51] Three references mention values of q which differ by several orders of magnitude, i.e., see Refs. 26, 28, and 29.
[52] A. De Wit and G. M. Homsy, J. Chem. Phys. **110**, 8663 (1999).
[53] J. Fernandez, P. Kurowski, P. Petitjeans, and E. Meiburg, J. Fluid Mech. **451**, 239 (2002).
[54] O. Manickam and G. M. Homsy, J. Fluid Mech. **288**, 75 (1995).
[55] J. Martin, N. Rakotomalala, and D. Salin, Phys. Fluids **14**, 902 (2002).
[56] T. Bánsági, Jr., D. Horváth, A. Tóth, J. Yang, S. Kalliadasis, and A. De Wit (preprint).